

Optimization of Wrap Angle in the Mixed Flow Impeller for Reducing Flow Losses

T. Prabu[†], P. Viswanathan, N. Gokul Kannan, R. Rudramoorthy and A. Firthouse

PSG College of Technology, Coimbatore, Tamil Nadu, 641004, India

[†]Corresponding Author Email: prabu.thangavel@gmail.com

(Received January 13, 2020; accepted May 25, 2020)

ABSTRACT

In this paper, mixed flow impeller is investigated to reduce the secondary flow loss and attain uniform flow at impeller exit by changing the wrap angle in the trailing edge (called as stacking condition). The 3D inverse design methodology is adopted for the blade profile generation using ADT Turbo suite software. The internal flow analysis of the base design is evaluated using commercial computational fluid dynamics (CFD). A single stage proto type model is tested and the experimental results have strong agreement with numerical analysis results. Further the impeller is designed with different wrap angle at the trailing edge of the hub and shroud region. The pump performance curve is obtained from numerical analysis for the optimized impellers from the ADT Turbo suite and compared with the base design. The wrap angle between 8° - 15° degree in hub region has the less secondary flow losses compared to the stacking in the shroud region. Higher wrap angle above 17° degree increases the diffusion ratio which in turn induces non-uniform flow at the impeller exit and also increases instability.

Keywords: Trailing edge; Inverse design; Computational fluid dynamics; Wrap angle.

1. INTRODUCTION

Submersible pumps are widely used in domestic and agriculture applications. The energy consumed by the pumps alone contribute to 20 % in the world's total electricity consumption (Hovstadius 2012). The existing pumps produced by world's leading manufacturing pump companies are operating in an efficiency of 40 -70 %. So the improvement in the pump energy efficiency will lead to greater saving on the energy bill as well as on environmental aspects.

Submersible pump consists of four major parts namely Impeller, diffuser, suction housing and non-return valve (NRV). Figure 1 shows the submersible pump and its parts. To improve the performance of the impeller, the secondary losses should be reduced by developing the proper internal flow path. Researchers all around the world are currently working on efficient internal flow path using various approaches like inverse design profile approach, stability parameter approach and geometrical modifications. The blade lean also known as stacking condition is considered to be an effective method to control the flow inside the impeller (Bonaiuti *et al.* 2010). Stacking condition

can be used to suppress secondary flow in centrifugal and mixed flow impellers (Yan *et al.* 2017). In this paper, the base impeller model is modified with the wrap angle trailing edge on the hub and shroud. The corresponding values of secondary losses and diffusion ratio are obtained from the turbo design software (Yan *et al.* 2016). The better performing models are investigated using computational fluid dynamics and the results are experimentally validated using experimental test setup.

2. GEOMETRY DESCRIPTION

The submersible pump and motor are coupled with the suction housing. Impeller is the rotating component that draws the fluid from the water table and transfer kinetic energy on the fluid by increasing pressure and velocity. The kinetic energy is converted into head with the help of diffuser and the fluid is diffused into the next stage. Non return valve prevents the reversal flow and also exhibits water hammer effect in the pump. In pumps, non-return valves supports to reduce the power consumption at the initial startup process and avoids the physical damage of pump due to water hammer effect.

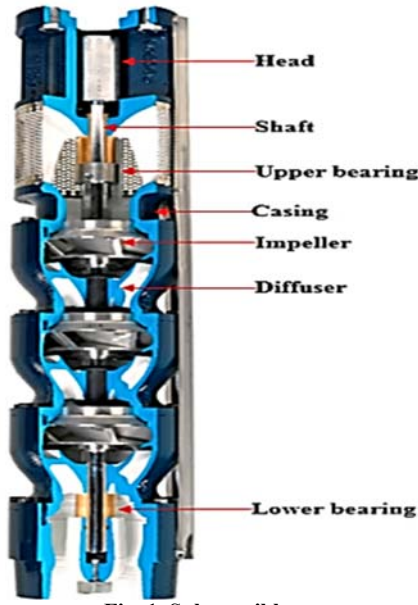


Fig. 1. Submersible pump.

In this work, submersible pump is designed for 6" inch bore size with the 58 (US) specific speed (N_s) of per stage as requested by the industrial experts based on the market research. Inverse methodology is adopted for the system design by using ADT turbo design software. The inverse blade loading is calculated based on the Eq. (1) shown below for impeller and diffuser (Yan *et al.* 2016).

$$p^+ - p^- = \frac{2\pi}{B} \rho W_{mb1} \frac{(rv\theta)}{\delta m} \quad (1)$$

(Where p^+ is pressure side of the blade, p^- is suction side of the blade, B number of blades, $rv\theta$ – pitch wise-averaged swirl velocity, W - Relative velocity, ρ – Density, δ - at the blade, m - Meridional direction)

The impeller and diffuser is designed with the combination of 6 and 7 backward curved blades respectively with 0° degree warp angle at trailing edge. The inbuilt numerical methods Eq. (2) in turbo design tool provides secondary flow losses and diffusion ratio in impeller as $4.48e^{-02}$ and 1.43 (Goto 2001; Zangeneh 1998) The base impeller is further designed for the different warp angle at the trailing edge of hub and shroud ranges from 0° to 20° .

$$W \cdot \nabla (W \cdot \Omega) = 2\Omega \cdot (W \cdot \nabla) W + \Omega (2\omega \times W) \quad (2)$$

(W - Relative velocity, ω - Rotational Speed, Ω – vorticity)

The base dimension arrived for the impeller are the inlet diameter $D_1 = 75$ mm, the outlet diameter $D_2 = 99$ mm, the exit width $b_2 = 15$ mm and with the original blade wrap angle of 0° . The basic parameters of the impeller are shown in Fig. 2 and Fig.3.

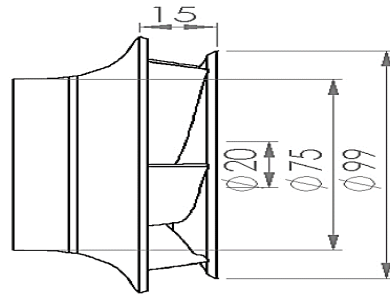


Fig. 2. Base impeller dimension.

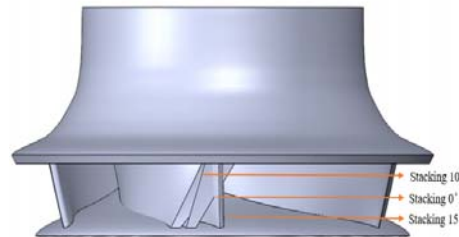


Fig. 3. Base impeller with stacking 10° , 15° .

During the stacking analysis the geometrical dimensions, blade thickness, load distributions and meridional flow path are kept unchanged. The wrap angle of base impeller with 10° Hub and 0° shroud region leads to stack warp angle of 10° is verified for flow losses in the Turbo design. The secondary flow and diffusion ratio is improvement from the base impeller. Figure 4 shows the impeller stacking validation method.

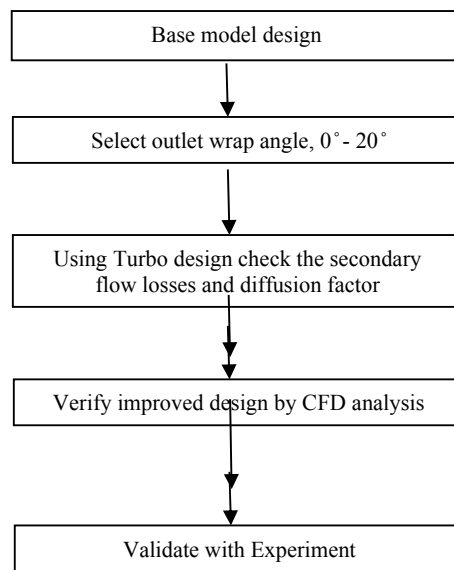


Fig. 4. Flow chart for impeller stacking validation.

Table 1 Stacking angle

Stacking	H 2	H 10	H 15	H 17.5	H 20	S2	S 10	S 20
Hub (angle in °)	2	10	15	17.5	20	0	0	0
Shroud (angle in °)	0	0	0	0	0	2	10	20

Further impeller is modified with 15° to 20° at the hub region and 0° shroud region for the wrap angles of 15° and 20°. The secondary flow loss has an improvement for the 15° wrap angle and deteriorates for the higher values as well there is no improvement on the diffusion ratio for all these cases. Then the impeller is modified with 0° at the hub region and 0° to 20° shroud region for the wrap angles of 10°, 15° and 20°. Figure 5 shows the various flow losses comparison of stacking. The variation by this approach has no significance on the performance improvement. The models with 0° shroud region with the wrap angles of 10°, 15° are considered for the simulation using commercial software Ansys CFX 18 to get the flow insight.

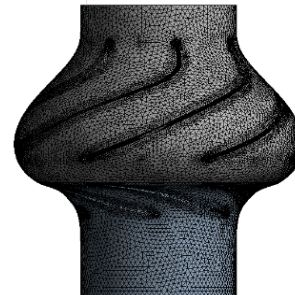


Fig. 6. Tetrahedral meshing.

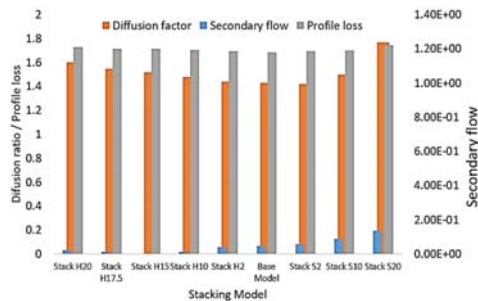


Fig. 5. Flow losses comparison of stacking.

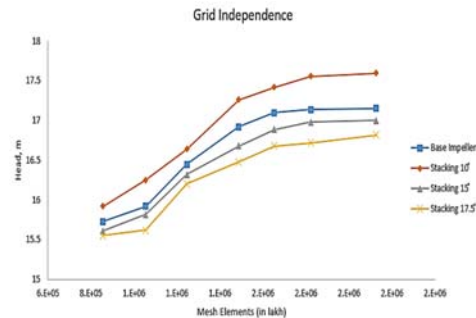


Fig. 7. Grid independency study.

3. COMPUTATIONAL METHODOLOGY

3.1 Mesh Independence

The Fluid model of single stage pump assembly consisting of impeller and diffuser fluid domain is taken for carrying out the analysis. The domain is discretized with the unstructured tetrahedral mesh for the ease of capturing the complex variation in the blades. As the flux variation is expected more near the wall, the blades are captured with refined small elements around the blades. The mesh quality is ensured for all the models. The grid-independence test was performed for single stage assembly with varying numbers of elements as shown in Fig. 6 to ensure the not much variation in head developed. The plot shown in figure depicts the number of elements versus the head variation and the head value is consistent and stable between 1.4 to 1.6 million elements. Figure 7 shows the grid independence study. Figure 8 and Fig. 9 shows the impeller and diffuser geometry respectively.



Fig. 8. Impeller.

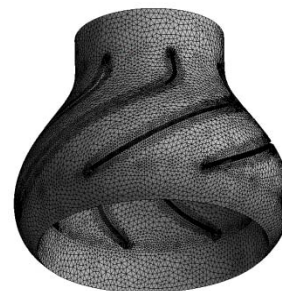


Fig. 9. Diffuser.

Table 2 Model setup

S.No	Solver	Options
1	Type	Pressure Based
2	Time	Steady
3	Viscous	K-ε Turbulence (RANS) Model
4	Interface	Frozen rotor

Table 3 Boundary conditions

S.No	Boundary Zones	Boundary Conditions	Values
1.	Inlet	Pressure Inlet	1 bar
2.	Outlet	Mass flow rate	0.2 Q _d - 1.6 Q _d
3.	Wall	Non slip & roughness	K5-1.1 Ra
4.	Impeller	Rotation speed	4000 RPM

3.2 Boundary Condition and Solver Setup

The impeller domain is rotating at the speed of 4000 rpm, whereas the diffuser domain remains stationary. Working fluid is defined as water with atmospheric condition. The model setup and the boundary conditions are given Table 2 & Table 3. Steady state incompressible flow with k-ε turbulence model (RANS) is used for the flow field in the CFX solver.

The numerical equations used for computational analysis are provided below. The second-order upwind scheme is applied for the momentum, turbulent kinetic energy and turbulent dissipation rate equations.

The Continuity equation & Momentum equation are given Eqs. 3& 4.

The continuity Equation

$$\frac{\delta \rho}{\delta t} + \nabla \cdot (\rho U) = 0 \quad (3)$$

(Where ρ – density, t – time, U – Velocity)

The Momentum Equations

$$\frac{\delta(\rho U)}{\delta t} + \nabla \cdot (\rho U \otimes U) = -\nabla p + \nabla \cdot \tau + S_M \quad (4)$$

Where the stress tensor,

$$\tau = \mu \left(\nabla U + (\nabla U)^T - \frac{2}{3} \delta \nabla \cdot U \right) \quad (5)$$

(Where ρ – density, t – time, U – Velocity, μ – viscosity, p- pressure, τ –shear stress)

$$\frac{\delta(\rho k)}{\delta t} + \nabla \cdot (\rho U k) = \nabla \cdot \left[\left(\mu + \frac{\mu_t}{\sigma_k} \right) \nabla k \right] + P_k - \rho \epsilon \quad (6)$$

$$\frac{\delta(\rho \epsilon)}{\delta t} + \nabla \cdot (\rho U \epsilon) = \nabla \cdot \left[\left(\mu + \frac{\mu_t}{\sigma_\epsilon} \right) \nabla \epsilon \right] + \frac{\epsilon}{k} (C_{\epsilon 1} P_k - C_{\epsilon 2} \rho \epsilon) \quad (7)$$

Where $C_{\epsilon 1}$, $C_{\epsilon 2}$, σ_k and σ_ϵ are constants.

P_k is the turbulence production due to viscous and buoyancy forces, which is modeled using:

$$P_k = \mu_t \nabla U \cdot (\nabla U + \nabla U^T) - \frac{2}{3} \nabla \cdot U (3\mu_t \nabla \cdot U + \rho k) + P_{kb} \quad (8)$$

3.3 Convergence Criteria

The residuals are scaled to fall below the values of 1×10^{-6} for the momentum and continuity equations for ensuring high stability in the off design conditions. The computational calculations are performed in parallel process workstation having 128 GB RAM & of clock speed 2.2 GHz which takes approximately 5 hours for 2000 iterations to provide every individual steady solution.

4. RESULTS AND DISCUSSION

4.1 Base Design

The computational analysis is carried out for flow rates ranging from 0.2 Q_d to 1.6 Q_d to study the performance of the base pump. The pressure and velocity plots obtained from the analysis are presented in Figs. 10 & 11. The static pressure variation from the impeller inlet to exit is smoothly varying at the higher mass flow condition of 1.6Q_d. The velocity distribution plots reveals the sudden change in velocity from impeller exit to diffuser inlet at the low mass flow condition. The pump performs during the designed flow condition and for the off design condition the performance drops due to the sudden changes in the flux as shown in Fig. 10. Figure 11 shows the stream line plot for the designed mass flow condition. As the kinetic energy is imparted over the fluid by rotating impeller, the streamline velocity is high in the impeller passage and then drops in the diffuser. The sudden jump from rotor to stator leads to energy loss and the passage is designed to reduce the losses by this approach.

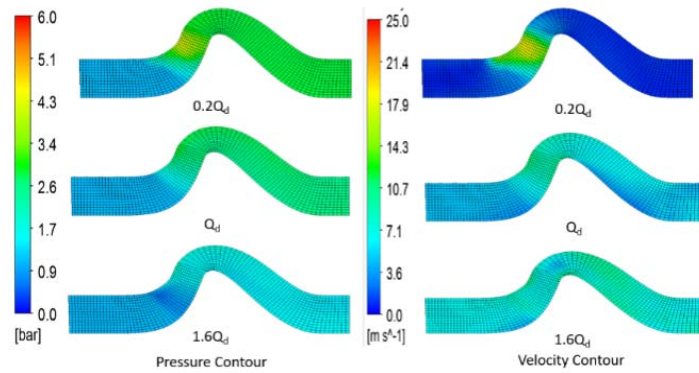


Fig. 10. Pressure and Velocity contours.

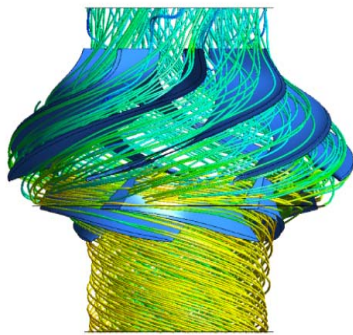


Fig. 11. Streamline flow path.

4.2 Rapid Prototype

The Stratasys FORTUS 900mc is an FDM 3D printer that runs on FDM Technology to build parts layer-by-layer from the bottom up by heating and extruding thermoplastic filaments. As the nozzle is moved over the table in the required geometry, it deposits a thin bead of extruded plastic to form each layer. The plastic hardens immediately after being squirted from the nozzle and bonds to the layer below. The entire system is contained within an oven chamber which is held at a temperature just below the melting point of the plastic.

The base model and optimized model are machined in the Stratasys FORTUS 900mc rapid proto type machine. The material used for proto type is ABS plastic. Figures 12 & 13 are the base design and impeller stacking angle of 10° . Initially, the surface roughness of ABS plastic about $0.8 - 1 \mu\text{m}$ is reduce to around $0.4 - 0.6 \mu\text{m}$ using conformal coating shows Fig.14.

4.3 Experiment and Validation

The pump is suspended from wooden rails placed at ground level into the well such that the inlet of the pump is submerged in water. A delivery pipe of 80mm diameter is used at the exit of the pump. A pressure tap to measure the delivery pressure is placed at length twice the diameter of delivery pipe from the exit of the pump. A gate valve is placed at length four time the diameter from the diameter of the pump. The flow meter is at ten diameter length

above the gate vale. The layout of the experimental setup is shown in Fig. 15 .The experimental testing shows Fig. 16 is carried out by varying flow rates to observe the characteristic of flow rate vs. head and respective pressure head is measured at the pump exit. The overall efficiency of the pump is obtained by measuring the fluid power and the electrical input power. The power input to the motor is measured using a power meter, which also provides with the voltage and current values. The speed of the motor is measures using a slip speed meter. The torque provided by the motor and pump input power is estimated using summation of losses method.

The results obtained from the numerical simulation and experimental tests are compared and it is deduced that the numerical simulation underestimates the head values in high flow rates while it overestimates the head values in lower flow rates. It is inferred from the underestimation of test results in low flow rates that the unsteady effects are not taken into consideration during steady calculations in the simulation.



Fig. 12. Base design.



Fig. 13. Impeller stacking 10° .



Fig. 14. Coated impeller.

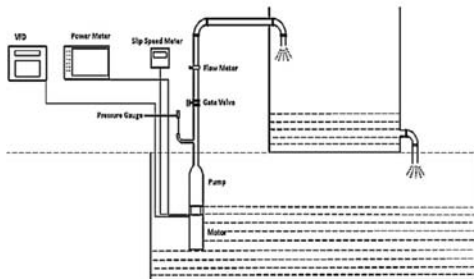


Fig. 15. Experimental setup.



Fig. 16. Single stage assembly.

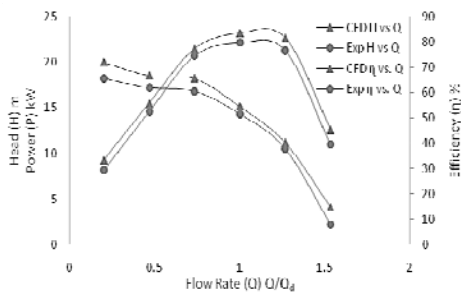


Fig. 17. Comparison of Flow rate with Head/Power & Efficiency.

In order to make the comparison of the total efficiency obtained from experiments and hydraulic efficiency η calculated by numerical simulations,

the ratio of total efficiency to the efficiency at design flow rate q/q_{dis} is introduced to minimize the effects of motor efficiency (Yan *et al.* 2015). The comparison of computational and experimental as shown in Fig.17 are in good agreement with head produced. The close agreement of computational and experimental results provides the confidence to proceed with the parametrical design optimization using the simulation.

4.4 Comparison of impeller design

The flow inside the impeller follows the blades with the flux variation on pressure side and suction side. At the tip of the blade the flow stream connects with the difference in the flux and leads to sudden change in the flow behavior. The blade angle at the tip plays a crucial role and will be controlled by the stack parameter. The effects of the stacking parameter at the trailing edge of the impeller is studied, Zangeneh (2010) a computational analysis is conducted for three best performing model namely stack H10, stack H15.

4.5 Variation of Pressure Gradient

The flow parameters are observed in three models with three different flow conditions. The Qd Stack H10 model performs well and the static pressure variation in the passage is smooth and achieving the higher head as shown in Fig. 18. It is observed in the Qd Base and Qd Stack15 models that the static pressure variation is uniform but the head developed is less compared with the Qd Stack H10. Under the design condition Qd, the pressure development in the impeller and pressure recovery in the diffuser is higher.

Pressure gradient at off design flow conditions in the impeller fluctuates more that is caused by the intense rotor-stator interaction of the impeller and the diffuser (Posa and Lippolis 2018). The head, power and efficiency curves for the flow rates ranging from 0.2 Qd to 1.6 Qd are shown in Fig. 19, 20 and 21. The head of stack H10 is greater than that of the base design and other two models in the design point.

The efficiency peaks at the designed flow condition for all the stacking models. It is observed that the head drops suddenly after 0.2 Qd in all models and the drop in magnitude for the stack H10 is comparatively less. This is due to the stacking effect provided by the impeller. Comparing all the three models, Stack H10 gives higher head with the highest efficiency in the minimum power consumption. The hydraulic efficiency at the design point 83%, and 87.5% for base design, stack H10 and stack H15 respectively from computational analysis.

4.6 Variation of Velocity

The velocity variation from impeller inlet to diffuser exit is observed in all the models. The velocity is gaining its magnitude when the impeller imparts the energy over fluid and drops while it is travelling

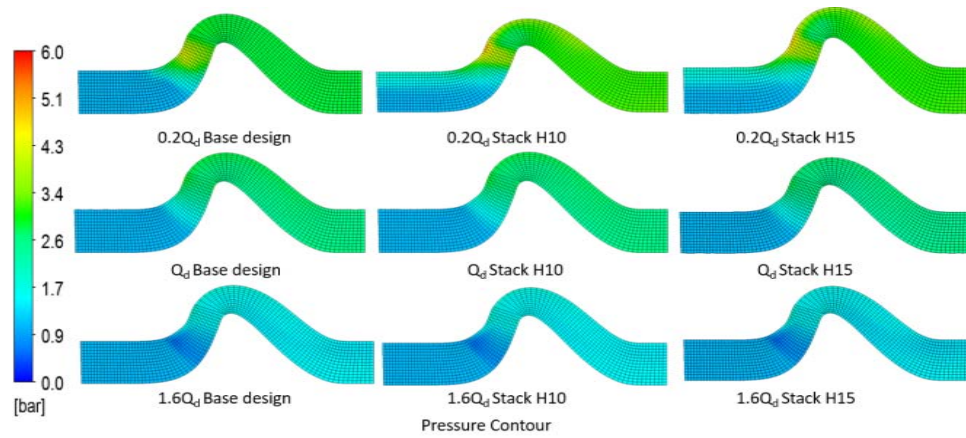


Fig. 18. Pressure contour comparison for various stack designs.

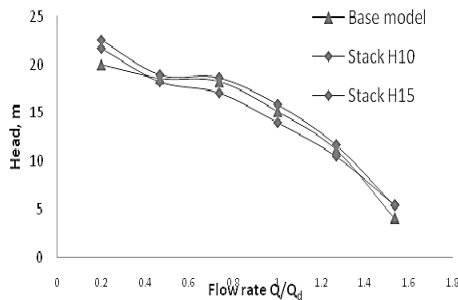


Fig. 19. Flow rate Vs. Pump head.

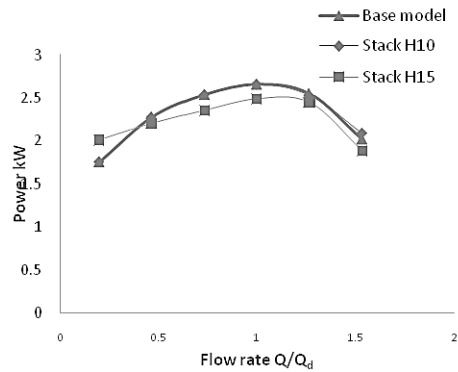


Fig. 20. Flow rate Vs Power.

over the diffuser as shown in Fig. 22. (Yang *et al.* 2012). It is observed that the main effect of the blade stacking is to suppress the secondary flow and Jet wake loss in the impeller and diffuser region (Bonaiuti *et al.* 2010).

The Fig 23 shows that the contours of velocity vector on the radial plane. It is observed that, in the base and stack H15 design, fluid detachment near the blade region is significantly higher comparing to the stack H10 model. This is due to the high secondary flow losses in both the designs. Therefore, the stack H10 model ensures the uniform

flow and stability in comparison to base & stack H15 model.

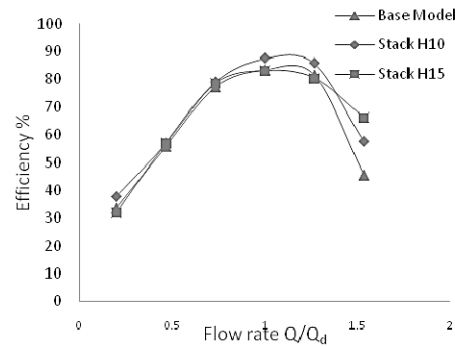


Fig. 21. Flow rate Vs. Efficiency.

4.7 Experimental Validation for Improved Design

The global variables of the pump are measured (flow rate) and in some cases estimated from measured quantities (head, efficiency). The net head produced by the machine is given by the difference in summation of the static head, dynamic head and potential head at the inlet and exit of the machine. The static head is measured by converting the pressure reading obtained from the pressure gauge to meters of water column.

$$H_p = \frac{P_{exit} \times 10^5}{\rho g} \quad (9)$$

Where, P_{exit} is the pressure transducer reading in bar, ρ is the density of water and g is the acceleration constant.

The velocity head is determined using the flow rate and the area of the delivery pipe. The expression for determining velocity head is given below.

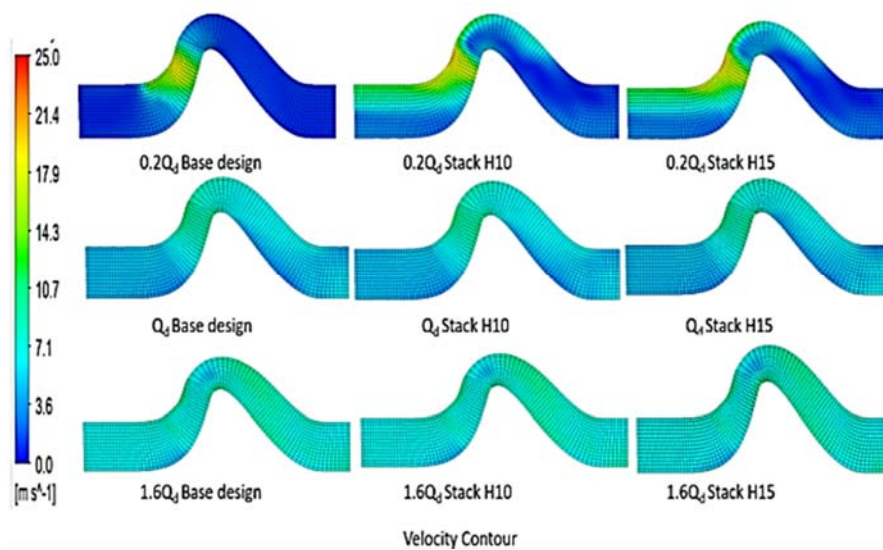


Fig. 22. Velocity contour comparison for various stack designs.

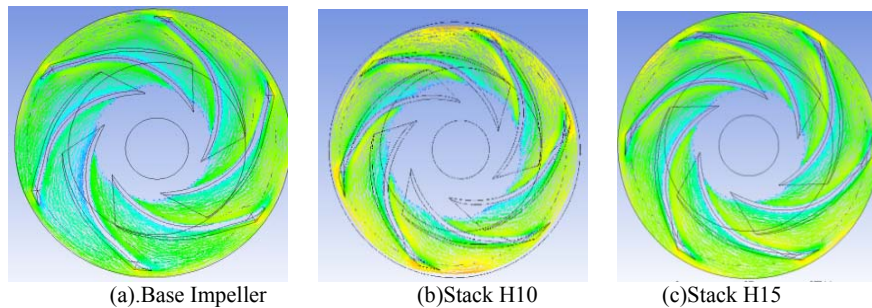


Fig. 23. Comparison of flow separation for different model at designed flow rate.

$$V = \frac{Q}{\frac{\pi \times d^2}{4}} \quad (10)$$

$$H_v = \frac{v^2}{2g} \quad (11)$$

Here, V is the velocity of the fluid in the delivery pipe, d is the diameter of the delivery pipe and Q is the flow rate measure.

The potential head due to the difference in elevation between the pump submergence level and the pressure gauge is accounted for by measuring the distance between the same (Z). The net head developed by the pump is given by the expression.

$$H = H_p + H_v + Z \quad (12)$$

The overall efficiency of the motor is given by the ratio of power developed by the pump to the input power to the motor. The power input to the motor (P_{in}), input voltage (V_{in}) and current (I_{in}) is measured using a power meter.

$$\eta_{\text{overall efficiency}} = \frac{\rho \times g \times Q \times H}{P_{in}} \quad (13)$$

It is observed that the stack design develops high pressure head with less power consumption

compared to the base design model under design flow rate conditions. Under low flow rate condition, both models are performed similarly but under high flow rate condition, stack H10 model more power compared to the base model. The head, efficiency, power curves for the flow rates ranging from 0.2 Qd to 1.6 Qd are shown in Figs. 24, 25 and 26.

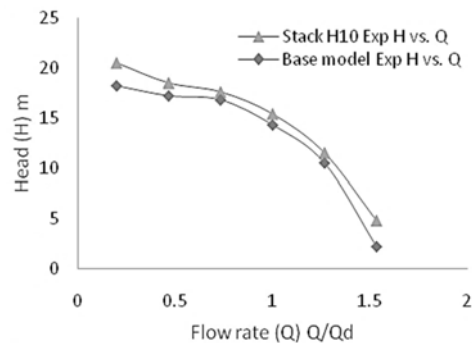


Fig. 24. Experimental head for base and Stack H10 model.

Table 4 Experimental comparison of model

Model	Head (m)	Power (kW)	η
Base	15.4	4.42	81.34
Stack H10	14.3	4.34	79.23

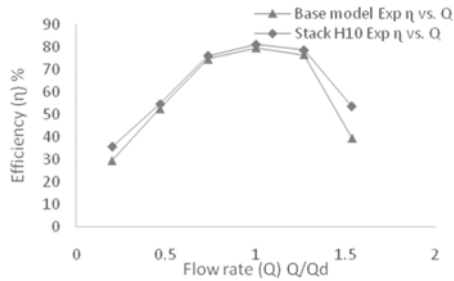


Fig. 25. Experimental Efficiency for base and Stack H10 model.

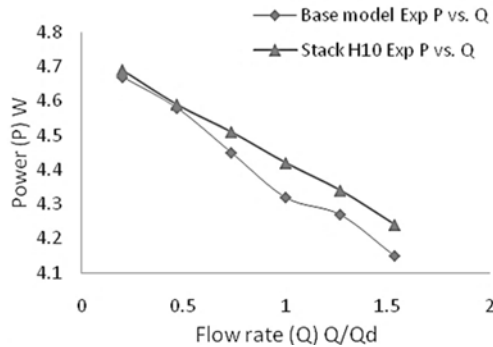


Fig. 26. Experimental head for base and stack H10 model.

5. CONCLUSION

In this study, centrifugal impeller with different wrap angle in the hub and shroud is optimized by ADT Turbo suite. Further the internal flow in the impeller and diffuser is investigated using CFD simulation. It is found that the wrap angle above 15° degree in the hub region increases the secondary flow and diffusion ratio leads to reduction in head compared to the base design. The wrap angle below 8° degree has less effect in the performance and is comparable with the base model performance. The wrap angle between 8° to 15° degree in the hub region is more effective in reducing the secondary flow, diffusion ratio. The stacking model H10 has the pump efficiency of 81.34% higher than the base design with efficiency 79.23 % which shows Table 4. The wrap angle in the shroud region has higher losses in the secondary flow and diffusion ratio.

ACKNOWLEDGEMENTS

This research was supported by the Department of Heavy Industries (DHI), New Delhi and Department of mechanical engineering, PSG College of Technology, Coimbatore.

REFERENCES

- Bonaiuti, D., M. Zangeneh, R. Aartojarvi and J. Eriksson (2010). Parametric design of a waterjet pump by means of inversedesign, CFD calculations and experimental analyse. *ASMEJ. Fluids Engineering* 132 (3) 031104.
- Goto, A. (2001, February). Optimization of pump blades using three dimensional inverse design methods. In *Proceedings of international Conference on Role of Advancements in Pump Technology in the Growth of Indian Economy*, Mumbai, India.
- Hovstadius, G. (2012). *Pump Systems Optimization – End User Training*. Industrial Energy Efficiency Project: Cape Town.
- Posa, A. and A. Lippolis (2018). A LES investigation of off-design performance of a centrifugal pump with variable-geometry diffuser. *International. Journal of Heat Fluid Flow* 70, 299–314.
- Yan, P. S. Li, S. Yang, P. Wu and D. Wu (2017). Effect of stacking conditions on performance of a centrifugal pump. *Journal of Mechanical Science and Technology* 31(2), 689–696.
- Yan, P., S. Li, S. Yang, P. Wu and D. Wu (2015). Effect of Trailing-EdgeModification of a Mixed-Flow Pump. *Journal of Fluids Engineering* 137(10), 101205.
- Yan, P., S. Li, S. Yang, P. Wu and D. Wu (2016). Computational Fluid Dynamics-Based Pump Redesign to Improve Efficiency and DecreaseUnsteady Radial Forces. *Journal of Fluids Engineering* 139(1), 011101.
- Yang, S. L., F. Y. Kong, H. Chen and X. H. Su (2012). Effects of blade wrap angel influencing a pump as turbine. *Journal of Fluid Engineering* 134, 1–8.
- Yumiko T. and H. Watanabe (2009). Multi-objective design optimization of a mixed-flow pump, *ASME Fluids Engineering Division Summer Meeting*, Vol 1:, Colorado, USA.
- Zangeneh, M. (1998). Optimization of Pump Blades Using Three Dimensional Inverse Design Method. *ASME Journal of Turbo Machinery* 120, 723-735.
- Zangeneh, M. (2010). Choice of optimum Blade loading in Application of 3D inverse Design to design of pump and Fans, *Proceeding of 2010 International Conference on Pumps and Fans*, China.